Assessing uncertainty in source rock properties using Monte Carlo basin modeling: Application to the Canning Basin, Australia

Jiayuan Huang[a*], Tapan Mukerji[a,b,c]

[a] *Department of Energy Science & Engineering, Stanford University, Stanford, California, USA*

[b] *Department of Earth & Planetary Sciences, Stanford University, Stanford, California, USA*

[c] *Department of Geophysics, Stanford University, Stanford, California, USA*

**jiayuanh@stanford.edu*

Abstract

This study presents a Monte Carlo basin modeling framework for quantifying uncertainty in source rock property predictions by integrating geological, geophysical, and geochemical inputs. The approach accounts for variability in petrological parameters from rock physics inversion, paleo-erosion magnitudes, organic facies properties, and boundary conditions to simulate source rock properties such as vitrinite reflectance, transformation ratio, temperature, and pore pressure. Application to the Goldwyer III unit in the Canning Basin, Australia, reveals that the source rock is within the oil to wet gas window, with substantial but incomplete transformation in the studied well locations. Sensitivity analysis identifies Cretaceous erosion and heat flow as the dominant controls on thermal maturity, while the transformation ratio is also strongly influenced by the hydrocarbon generation kinetics model. Comparison with rock physics inversion and T_{max}-based maturity calculations demonstrates that Monte Carlo basin modeling significantly reduces

uncertainty by incorporating geological constraints and process-based modeling. This integrated framework improves the reliability of source rock property assessments and offers a valuable tool for exploration risk reduction.

Keywords: Uncertainty quantification; Monte Carlo simulation; Basin and Petroleum System modeling; Unconventional shale; Thermal maturity; Source rock properties; Canning Basin

1 Introduction

Quantifying the thermal and burial evolution of sedimentary basins is essential for understanding petroleum system development and assessing exploration risk. Rock physics inversion is a powerful tool for estimating subsurface source rock properties from well logs or seismic data. However, key properties such as thermal maturity, transformation ratio, and pore pressure are difficult to infer accurately through rock physics inversion alone. To address this challenge, basin and petroleum system modeling (BPSM) integrates geological, geochemical, and geophysical data to simulate the processes that control hydrocarbon generation, migration, and accumulation over geological time (Hantschel & Kauerauf, 2009). Despite its strengths, BPSM still relies on numerous input parameters including paleo-heat flow, erosion magnitudes, organic facies properties, and kinetic models that are inherently uncertain due to limited data availability, spatial variability, and interpretational ambiguities.

Traditional basin models are often constructed using deterministic input values, which may oversimplify the range of geological scenarios, lead to misleading predictions of source rock maturity, hydrocarbon generation, and reservoir quality, and may not assess the associated uncertainties of the predictions. Recognizing and quantifying these uncertainties is crucial for making more robust geological interpretations and for guiding exploration decisions (Peters et al., 2012).

Monte Carlo simulation provides a powerful framework for addressing input uncertainties in basin modeling by treating key parameters as probability distributions rather than fixed values. Through stochastic sampling and multiple model realizations, Monte Carlo basin modeling can capture the range of possible geological outcomes and provide probabilistic assessments of thermal histories, hydrocarbon generation timing, and petroleum system efficiency. Brevik et al. (2014) introduced the term geophysical basin modeling (GBM) to describe the process of estimating velocity models by integrating rock physics with basin modeling results. Tong and Mukerji (2017) implemented Monte Carlo basin modeling combined with sensitivity analysis to identify the impact of uncertain parameters on both spatial and temporal model responses. Tømmerås et al. (2018) employed an iterative Monte Carlo basin-modeling workflow that probabilistically calibrates uncertain input parameters by weighting the misfit between observed and modeled oil- and gas-column heights. More recently, Fonseca et al. (2023) proposed Bayesian geophysical basin modeling (BGBM), which integrates geological data, physical modeling, and geologic knowledge through Monte Carlo simulation and Bayesian inference to quantify uncertainty for pore pressure prediction in sedimentary basin models.

In this study, we apply a Monte Carlo-based basin modeling workflow to the Goldwyer III unit in the Canning Basin (Western Australia) to quantify uncertainty for important source rock properties. Key geological uncertainties, including source rock lithology, organic-facies properties, kinetic models, erosion magnitudes, heat flow history, are treated as stochastic variables. A total of 500 basin models were generated using PetroMod, with inputs sampled from defined probability distributions based on well data, geochemical analyses, rock physics inversion, and regional geological interpretations. The simulation results are used to evaluate the range of source rock properties such as hydrocarbon generation potential, temperature, pressure, and associated uncertainties in the Goldwyer III unit.

2 Geologic setting and study area

2.1 Regional geological framework

The Canning Basin, located in northwestern Australia, is one of the largest and least explored sedimentary basins in the world (Kuuskraa et al., 2013). It is a large Paleozoic basin characterized by a thick and relatively underexplored stratigraphic succession. Deposition within the basin includes major episodes of evaporite formation followed by salt tectonism, an extensive succession of Devonian reef facies, and repeated phases of continental to marine shelf sedimentation in an intracratonic setting (D'Ercole et al., 2003). The Canning Basin hosts multiple proven and potential petroleum systems (Schenk et al., 2018).

2.2 Stratigraphy and source rock characteristics

The study area is in the Broome platform, where the Ordovician Willara, Goldwyer and Nita Formations have good hydrocarbon potential (Ghori et al., 2007; Haines, 2004) (Figure 1). In this work, we focus on the Goldwyer III unit, which represents the principal source rock in the region. The Goldwyer Formation is a Lower to Middle Ordovician organic-rich marine shale deposited in an open marine environment (Cadman et al., 1993; Haines, 2004). Depositional facies indicate alternating water depths, ranging from quiet subtidal or lagoonal conditions to higher-energy shoal and intertidal settings, reflecting two broad cycles of relative deepening and subsequent shallowing during Goldwyer deposition (Haines, 2004). The formation is subdivided into upper shale unit (Goldwyer I), middle carbonate unit (Goldwyer II), and lower shale unit (Goldwyer III) (Foster et al., 1986). In this study, we focus on the Goldwyer III unit which is the primary source rock in this area. The Goldwyer III unit exhibits high total organic carbon (TOC) and predominantly oil-gas-prone Type II-III and gas-prone Type III kerogen, making it one of the most significant source rocks in the basin (Johnson et al., 2020; Iqbal et al., 2022). The burial and thermal evolution of this interval, which drives its present-day maturity, is further influenced by the basin's tectonic history, discussed in the following subsection.

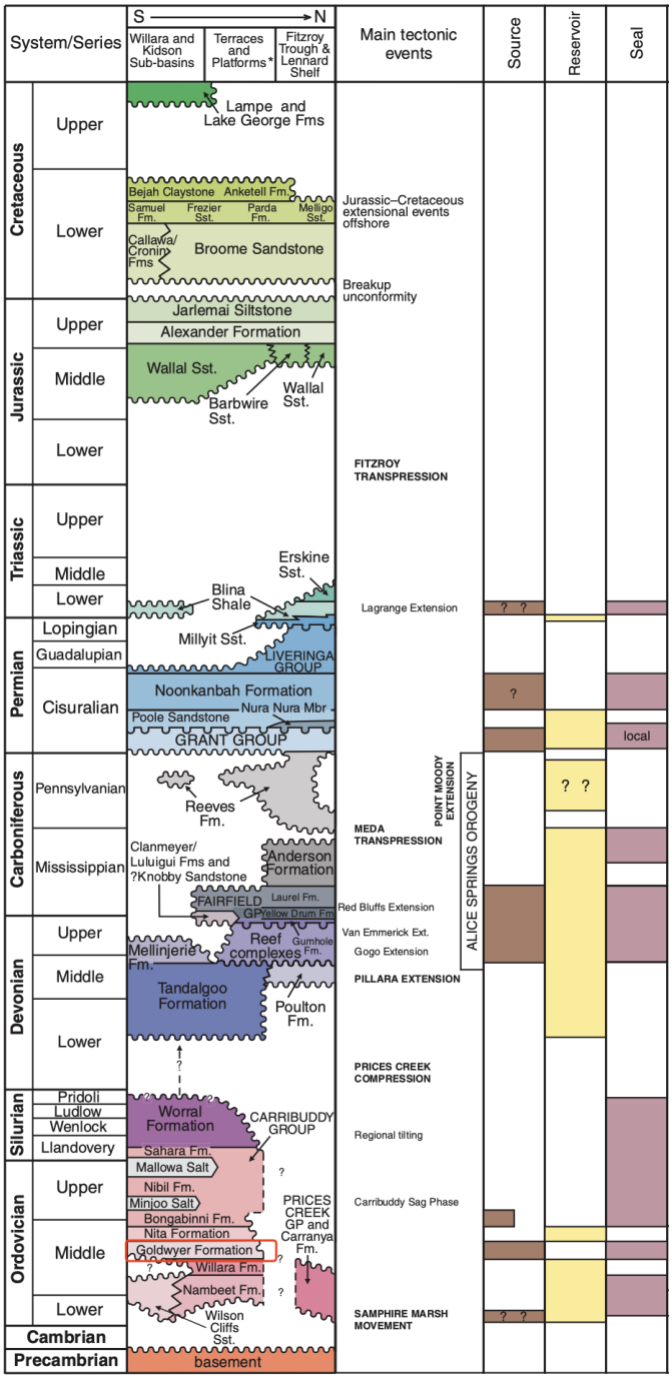

Figure 1. Generalized stratigraphy and main tectonic events of the Canning Basin (Modified from Haines, 2011).

2.3 Tectonic history

The tectonic history of the Canning Basin includes several major deformation phases, including the Samphire Marsh extension (Ordovician–Silurian), Prices Creek compression (Devonian–Carboniferous), Meda transpression (Carboniferous–Triassic), Fitzroy transpression (Triassic–Jurassic), and Jurassic–Cretaceous extension (Ghori et al., 2007; Haines, 2011) (Figure 1). These tectonic events generated regional unconformities, uplift, and variable subsidence rates, which significantly influenced the burial depth, thermal regime, and maturity of the Ordovician source rocks. More detailed descriptions of the tectonostratigraphic evolution of the basin can be found in Brown (1984) and Garcia (2014).

In this study, the tectonic history directly constrains the basin thermal history and burial model, which are used to simulate temperature evolution and consequently control vitrinite reflectance and kerogen transformation. Incorporating tectonic events into the burial and heat-flow reconstruction is therefore essential for obtaining realistic thermal maturation histories and ensuring that the basin modeling results are geologically consistent.

2.4 Locations of well and seismic survey

Theia-1 is the key well used in this study and is located within the Goldwyer III depocenter of the Canning Basin (Figure 2). The well lies close to the Carribuddy seismic survey line that intersects the study area, providing structural and stratigraphic context for the Goldwyer Formation. A pre-stack seismic inversion section is available along this line and ties directly to the Theia-1 well, enabling well-to-seismic correlation across the survey area.

Figure 2. Locations of well and seismic survey in the Canning Basin. Red dots indicate well location while the blue curve represents the 2-D seismic section.

3. Limitations of rock physics inversion and motivation for basin modeling

In our previous study, statistical rock physics inversion was applied using the elastic properties from Carribuddy seismic survey and Theia-1 well to estimate key source rock properties within the Goldwyer III unit (Huang et al., 2025). The inversion followed a Bayesian inference framework, where prior distributions of vitrinite reflectance, porosity, kerogen content, and mineral composition were defined from geological knowledge, and elastic properties were forward-modeled using a thermal-maturation–dependent rock physics model (Al Ibrahim et al., 2020). The statistical distance between modeled and observed elastic properties (V_P, V_S, and density) was then used to update the prior distributions through weighted Approximate Bayesian Computation (ABC), yielding posterior estimates of the source rock properties.

The inversion successfully constrained porosity, kerogen content, and clay content, as evidenced by clear posterior updating relative to the priors. However, vitrinite reflectance showed minimal posterior change (Figure 3), indicating that well-log derived and seismic-derived elastic properties have limited sensitivity to thermal maturity. This highlights a fundamental limitation of rock physics inversion: while effective at constraining elastic and compositional parameters, it is generally not well suited for estimating properties that are primarily controlled by burial and thermal history.

To overcome this limitation, we introduce a Monte Carlo basin modeling approach, which explicitly incorporates geologic processes such as sedimentation, erosion, heat flow, and kerogen kinetics to estimate thermal maturity (vitrinite reflectance) and related outputs probabilistically.

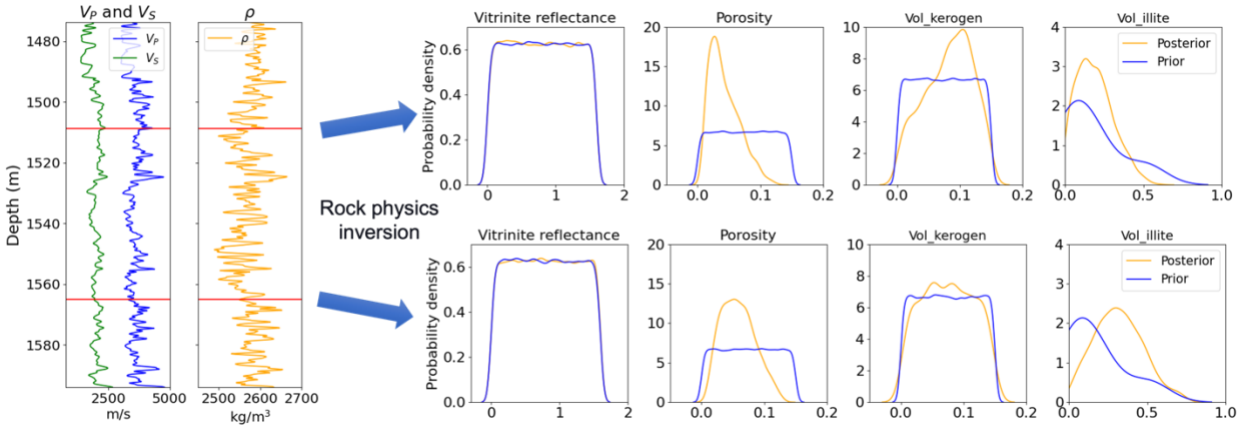

Figure 3. Prior and posterior distributions from the statistical rock physics inversion for the Goldwyer III unit. In this Bayesian inference framework, the prior distributions are defined from geological knowledge and reflect the initial uncertainty before conditioning on elastic properties from well log or seismic data. The posterior distributions incorporate information extracted from elastic properties through the inversion. Clear shifts from prior to posterior are observed for

porosity, kerogen content, and mineral composition, indicating that these properties are constrained by the elastic properties. In contrast, vitrinite reflectance shows almost no change between its prior and posterior distributions, demonstrating that elastic properties alone are insufficient to constrain thermal maturity in this dataset (Huang et al., 2025).

4. Methods

Basin modeling requires a range of geological and geophysical inputs, including stratigraphy, lithology, paleo-water depth, heat flow history, erosion events, and geochemical parameters such as hydrogen index (HI) and kerogen kinetics. These inputs can be derived from the rock physics inversion, laboratory measurements, well logs, stratigraphic interpretations, and tectonic history, and are integrated into a Monte Carlo framework to quantify uncertainty and explore the range of possible source rock properties that cannot be reliably constrained through rock physics inversion alone.

4.1 Proposed workflow

In this study, Monte Carlo basin modeling is applied to estimate source rock properties that cannot be directly inferred from rock physics inversion using elastic properties derived from well logs and seismic data (Figure 4). The posterior distributions of key source rock properties, including kerogen content, porosity, and mineral compositions, are randomly sampled to construct the source rock formation input for basin modeling. Well logs are utilized to estimate paleo-erosion and infer kinetics and the hydrogen index (HI) of the organic facies. Boundary conditions, such as paleo

water depth (PWD), sediment-water interface temperature (SWIT), and heat flow (HF), are constrained using biostratigraphy and regional tectonic history. Multiple realizations of basin models are then generated and used in the simulations. The Monte Caro basin modeling outputs include thermal maturity (%R_o), temperature, transformation ratio (TR), fluid saturation, permeability, and pressure, providing insights into the uncertainties associated with the source rock system.

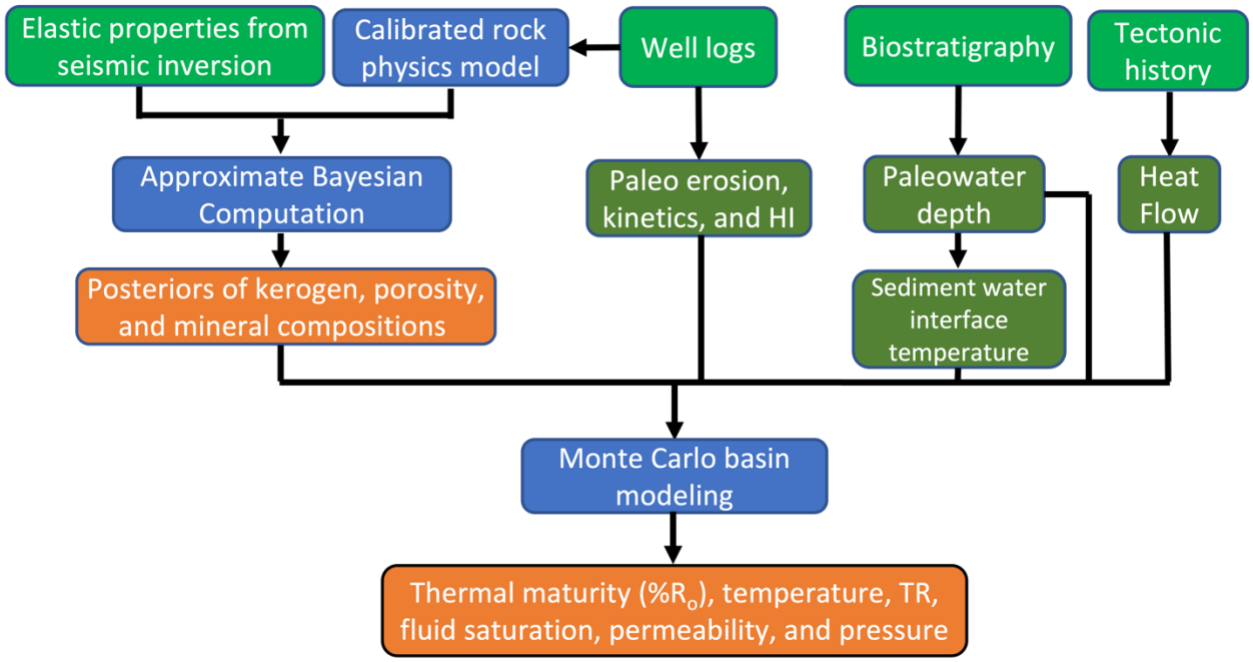

Figure 4. Proposed workflow of Monte Carlo basin modeling. TR is transformation ratio; HI is hydrogen index.

4.2 Monte Carlo basin modeling

The Stanford Basin and Petroleum System Modeling (BPSM) PetroMod Toolbox for MATLAB is used to automate multi-model construction and simulation (Al Ibrahim, 2019) in the commercial PetroMod basin modeling software. The workflow of the toolbox is as follows (Figure 5):

1. Build a template model using the PetroMod graphical user interface (GUI).
2. Define parameters (e.g., lithology, hydrogen index (HI), boundary conditions, etc.) and their probability distributions for Monte Carlo sampling.
3. Generate multiple basin models by duplicating the template and modifying its parameters based on Monte Carlo samples.
4. Execute simulations for all the basin models.
5. Load the simulation results from all the models.
6. Analyze the simulated results for further interpretation.

Steps 3, 4, and 5 are independent for each model, allowing them to be executed in parallel to significantly reduce computational time.

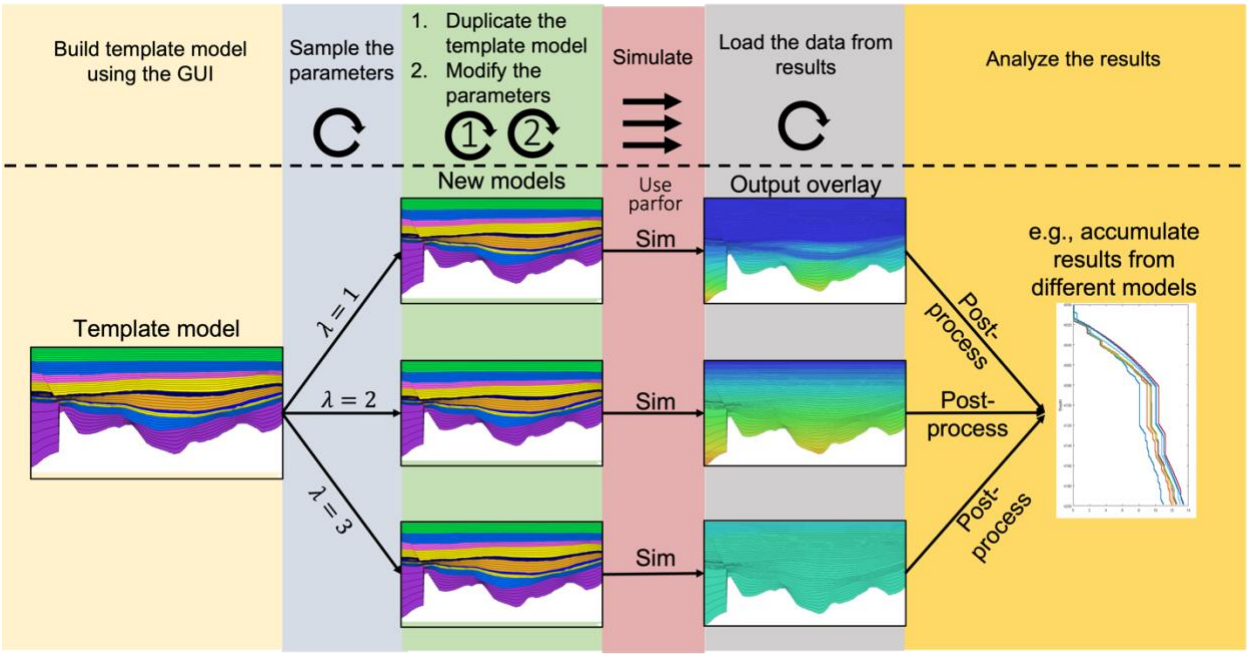

Figure 5. Workflow for the Stanford BPSM PetroMod Toolbox for MATLAB (modified from Al Ibrahim, 2019).

5. Monte Carlo basin modeling inputs and data

The inputs for the Monte Carlo basin modeling begins with 1D basin model template and then details the estimation of key uncertain parameters, including petrological properties, paleo-erosion magnitudes, organic facies characteristics, and boundary conditions. Finally, a summary of the Monte Carlo sampling strategy is provided.

5.1 Input table of 1D basin model template

In this study, a 1D basin model template serves as the foundational structure for Monte Carlo basin modeling. The input table of the template provides the fundamental geological, geochemical, and thermal properties required for basin modeling. These values act as baseline inputs for the simulation and include formation depths, ages, erosion estimates, organic facies properties, and thermal boundary conditions. The input table consolidates data from well logs, seismic inversion, geochemical analysis, and regional geological studies, ensuring a realistic representation of the subsurface system.

Monte Carlo simulations are then applied by randomly sampling uncertain parameters, duplicating the template models, and replacing the corresponding values in each duplicated template model. This process generates multiple realizations of the basin model, allowing for a comprehensive

uncertainty analysis of key basin parameters, such as thermal history and hydrocarbon generation potential.

A basin model template used in this study is prepared based on the stratigraphy in Figure 1 and is shown in Table 1.

Table 1. 1D basin model template. The variables with green color will be sampled during the Monte Carlo simulation (Modified from Johnson et al., 2020).

Age (Ma)	Formation	Depth (m)	Thickness (m)	Event type	Paleodeposition/ Erosion (m)	Lithology	PSE	Kinetic	TOC (wt. %)	HI (mg/g TOC)
0	Recent	0	10	Deposition		Sandstone (typical)	Overburden Rock			
70	Broome Sandstone	10	30	Deposition		Sandstone (typical)				
100	Cretaceous Erosion	40	0	Erosion	Erosion_1					
150	Jarlemai Silstone	40	125	Deposition	Deposition_1	Siltstone (organic lean)				
165	Wallal Sandstone	165	76	Deposition		Sandstone (typical)	Reservoir Rock			
250	Lower Triassic Erosion	241	0	Erosion	Erosion_2					
280	Grant Formation	241	600	Deposition	Deposition_2	Sandstone (typical)				
360	Hiatus L. Devonian	841	0	Hiatus						
436	Carribudy Formation	841	137	Deposition		Shale (typical)	Overburden Rock			
450	Bongabinni Formation	978	41	Deposition		Dolomite (typical)	Seal Rock			
455	Nita Formation	1019	169	Deposition		Siltstone (organic lean)	Reservoir Rock			
463	Goldwyer I	1188	178	Deposition		Shale (organic rich, 3% TOC)	Source Rock	Pepper&Corvi(1995)_TII(B)	4	700
465	Goldwyer II	1366	106	Deposition		Limestone (organic rich - typical)				
475	Goldwyer III_1	1472	7	Deposition		Lithology_1	Source Rock	Kinetic_1	TOC_1	HI_1
475.29	Goldwyer III_2	1479	7	Deposition		Lithology_2	Source Rock	Kinetic_2	TOC_2	HI_2
475.59	Goldwyer III_3	1486	7	Deposition		Lithology_3	Source Rock	Kinetic_3	TOC_3	HI_3
475.88	Goldwyer III_4	1493	7	Deposition		Lithology_4	Source Rock	Kinetic_4	TOC_4	HI_4
476.18	Goldwyer III_5	1500	7	Deposition		Lithology_5	Source Rock	Kinetic_5	TOC_5	HI_5
476.47	Goldwyer III_6	1507	7	Deposition		Lithology_6	Source Rock	Kinetic_6	TOC_6	HI_6
476.76	Goldwyer III_7	1514	7	Deposition		Lithology_7	Source Rock	Kinetic_7	TOC_7	HI_7
477.06	Goldwyer III_8	1521	7	Deposition		Lithology_8	Source Rock	Kinetic_8	TOC_8	HI_8
477.35	Goldwyer III_9	1528	7	Deposition		Lithology_9	Source Rock	Kinetic_9	TOC_9	HI_9
477.65	Goldwyer III_10	1535	7	Deposition		Lithology_10	Source Rock	Kinetic_10	TOC_10	HI_10
477.94	Goldwyer III_11	1542	7	Deposition		Lithology_11	Source Rock	Kinetic_11	TOC_11	HI_11
478.24	Goldwyer III_12	1549	7	Deposition		Lithology_12	Source Rock	Kinetic_12	TOC_12	HI_12
478.53	Goldwyer III_13	1556	7	Deposition		Lithology_13	Source Rock	Kinetic_13	TOC_13	HI_13
478.82	Goldwyer III_14	1563	7	Deposition		Lithology_14	Source Rock	Kinetic_14	TOC_14	HI_14
479.12	Goldwyer III_15	1570	7	Deposition		Lithology_15	Source Rock	Kinetic_15	TOC_15	HI_15
479.41	Goldwyer III_16	1577	7	Deposition		Lithology_16	Source Rock	Kinetic_16	TOC_16	HI_16
479.71	Goldwyer III_17	1584	9	Deposition		Lithology_17	Source Rock	Kinetic_17	TOC_17	HI_17
480	Willara Formation	1593	53	Deposition		Limestone (shaly)				
489	Nambeet Formation	1646								

5.2 Key uncertain parameters and their estimation

Paleo-erosion plays a critical role in basin modeling by influencing the burial history, thermal evolution, and maturation of source rocks. Significant erosion events can remove substantial overburden, thereby reducing the burial depth and altering the thermal regime of the basin over

time (Allen and Allen, 2013). Accurately estimating the magnitude and timing of these erosion events is essential for reconstructing realistic burial and temperature histories.

Organic facies properties are essential inputs for basin modeling, as they govern the timing, quantity, and type of hydrocarbon generation during the thermal evolution of a source rock (Peters and Cassa, 1994). Key properties include hydrogen index (HI), kerogen type, and hydrocarbon generation kinetic model (e.g., activation energy and frequency factor), all of which influence the transformation of organic matter into hydrocarbons under varying burial and thermal conditions.

Basin modeling requires thermal boundary conditions at both the top and base of the sedimentary column. The top thermal boundary condition is the paleosurface temperature, estimated based on paleolatitudes and paleo water depth (PWD) through geologic time (Hsu and Robinson, 2017). In the simulation software, this paleosurface temperature is referred to as the sediment-water interface temperature (SWIT).

5.2.1 Petrological inputs estimated from rock physics inversion

Distributions of petrological inputs including lithology, porosity, and TOC are estimated using the statistical rock physics inversion method from Huang et al. (2025). In this Bayesian framework, the posterior distributions represent the updated probability distributions of petrophysical properties after integrating prior geological knowledge with the observed seismic or well-log elastic properties data. These posterior samples quantify uncertainty and are used as geologically consistent inputs for Monte Carlo basin modeling. In this study, a 1D vertical column is extracted from the 2D inversion results. This column, located within the Goldwyer III unit, is discretized

into N layers (with N = 17 near the Theia-1 well). At each layer, porosity values are randomly sampled and used to approximate Athy's compaction factor (Athy, 1930) for modeling mechanical compaction. Total organic carbon (TOC) values are resampled from the posterior distribution of kerogen volume fractions obtained through rock physics inversion and converted to weight percent by dividing by two, assuming a kerogen-to-bulk rock density ratio of approximately 1:2 (i.e. assuming kerogen density ≈1.3 g/cm^3 (Al Ibrahim, 2019) and bulk rock density ≈2.6 g/cm^3). Six mineral components from rock physics inversion—quartz, calcite, illite, chlorite, dolomite, and pyrite—are randomly sampled from their respective posterior distributions. Lithology is then represented by these six minerals using the mixing function in the Lithology Editor of PetroMod. The workflow is shown in Figure 6.

The distributions of porosity and TOC are modeled using kernel density estimation (KDE) based on the posterior samples obtained from the rock physics inversion, while the distributions of mineral compositions are modeled using Dirichlet distributions to ensure that the sampled fractions sum to one (MacKay, 2003). The Dirichlet parameters are estimated via maximum likelihood based on the inversion results (Minka, 2000).

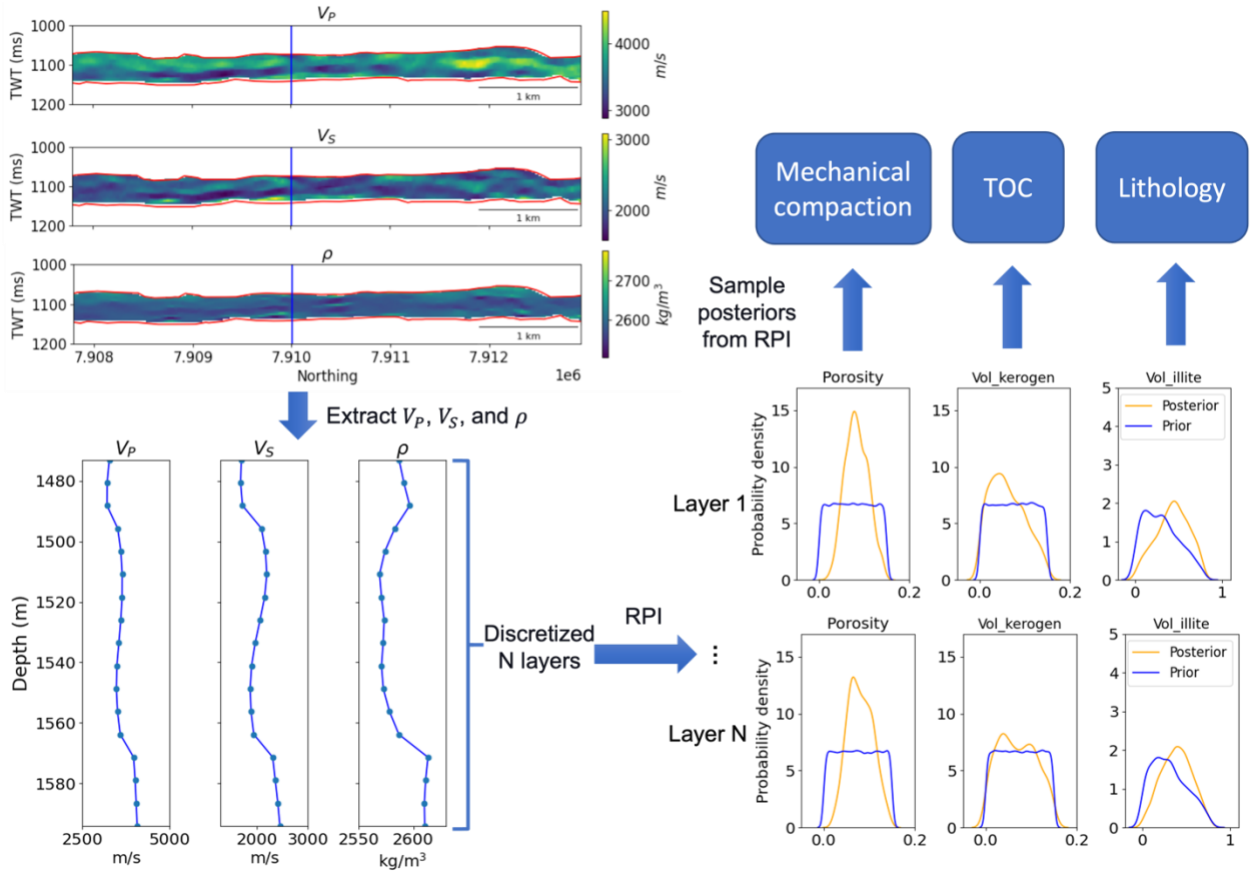

Figure 6. Workflow for sampling posterior distributions from rock physics inversion results to estimate mechanical compaction and petrological inputs for the basin model. The prior represents the initial probability distribution of each petrophysical property based on geological knowledge before incorporating geophysical observations, while the posterior represents the updated distribution after integrating seismic or well-log elastic data through Bayesian inference. The posterior samples of porosity, TOC, and mineral fractions are used as inputs for Monte Carlo basin modeling. RPI is rock physics inversion. TOC is total organic carbon.

5.2.2 Paleo-erosion estimates

307 Johnson et al. (2017) estimated erosion magnitude using sonic transit time data and erosion
308 magnitudes at eight wells were estimated, as listed in Table 2. For each well, the results are
309 reported as a lower 95% confidence limit, an upper 95% confidence limit, and a maximum
310 likelihood estimate. The erosion magnitude at the Theia-1 well was then approximated by linearly
311 interpolating the values from the four geographically closest wells in the study area (highlighted
312 in Table 2).
313
314 Table 2. Estimation of erosion from Broom Platform wells (Johnson et al., 2019). The values are
315 lower 95% confidence limit, upper 95% confidence limit, and maximum likelihood estimate,
316 respectively. The first eight wells are from Johnson et al. (2019). The highlighted four wells are
317 used for estimating the erosion of Theia-1 well.
318

Well Name	Sections	
	Jurassic-Cretaceous (m)	Carboniferous-Permian (m)
Hilltop-1	400-2100 (1600)	500-2000 (1400)
Aquila-1	800-1900 (1400)	500-2200 (1300)
McLarty-1	200-1200 (800)	1000-2000 (1700)
Kunzea-1	400-800 (500)	200-1800 (900)
Musca-1	600-2000 (1200)	300-1500 (1200)
Matches Springs-1	400-1300 (1000)	300-900 (600)
Santalum-1	900-2000 (1800)	No Records
Edgar Range-1	300-2100 (1000)	200-1700 (1400)
Theia-1 (Estimated)	450-2046 (1109)	267-1706 (1330)

To represent uncertainty in paleo-erosion at the Theia-1 location, we model the erosion magnitudes for the Jurassic–Cretaceous and Carboniferous–Permian periods using truncated normal distributions (Virtanen et al., 2020). In this formulation, the maximum likelihood estimate is used as the mean, and the lower and upper 95% confidence limits define the minimum and maximum bounds of the distribution (Figure 7). This approach captures both the central tendency and the plausible uncertainty range while preventing unrealistic erosion values outside the confidence interval.

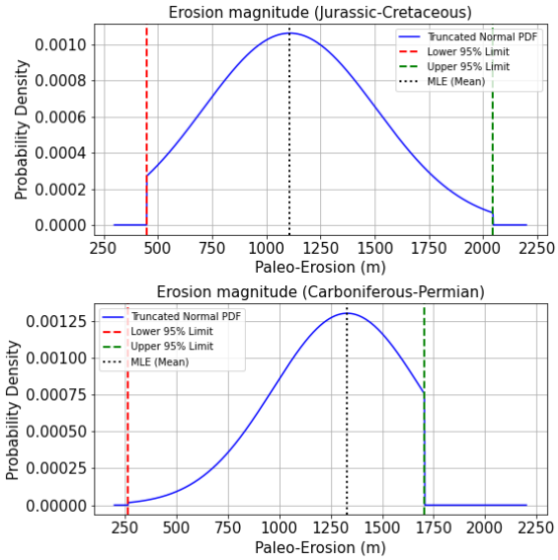

Figure 7. Truncated normal distributions of paleo-erosion magnitudes during the Jurassic–Cretaceous and Carboniferous–Permian periods at the Theia-1 well. The mean is defined by the maximum likelihood estimate, and the lower and upper bounds correspond to the 95% confidence limits derived from nearby wells (Johnson et al., 2019; Virtanen et al., 2020).

5.2.3 Organic facies properties

In this study, we compiled Rock-Eval pyrolysis data from the Theia-1 well, including HI and kerogen type, from Johnson et al. (2020) and Iqbal et al. (2022). The HI values range from 60 to 268 mg HC/g TOC, and the distribution is modeled using KDE. Kerogen within the Goldwyer III unit is classified primarily as Type II–III and Type III (Peter & Cassa, 1994). Johnson et al. (2020) demonstrated that the Pepper and Corvi (1995) default kinetics for Type II kerogen in PetroMod most closely match the experimental kinetic results for Type II/III within the Goldwyer III unit. Therefore, for modeling purposes, we randomly sample kinetic models from the PetroMod default Type II kinetics for Type II–III kerogen, and from the Type III default kinetics for samples classified as Type III (Pepper & Corvi, 1995).

The distribution of kinetic models within the Goldwyer III unit is constructed and sampled using a Discrete-Time Markov Chain (DTMC; Norris, 1998) to account for spatial correlation and transition dependencies between adjacent layers. Without DTMC, kinetic model assignments would rely on independent random sampling, ignoring geological continuity and potentially producing unrealistic vertical heterogeneity. DTMC allows us to model the likelihood that a given layer's kinetics resemble those of adjacent layers, reflecting stratigraphic trends and improving geologic realism in the generated realizations. The transition probability matrix is estimated by computing empirical frequencies of kinetic model transitions observed in well log interpretations across the unit and is summarized in Table 3. The actual data histogram and modeled distribution of Hydrogen Index (HI) using KDE based on the available HI dataset are shown in Figure 8.

Table 3. Transition probability matrix used in the DTMC model to represent the spatial distribution of kerogen types within the unit.

	Type II-III	Type III
Type II-III	0.9	0.1
Type III	0.1	0.9

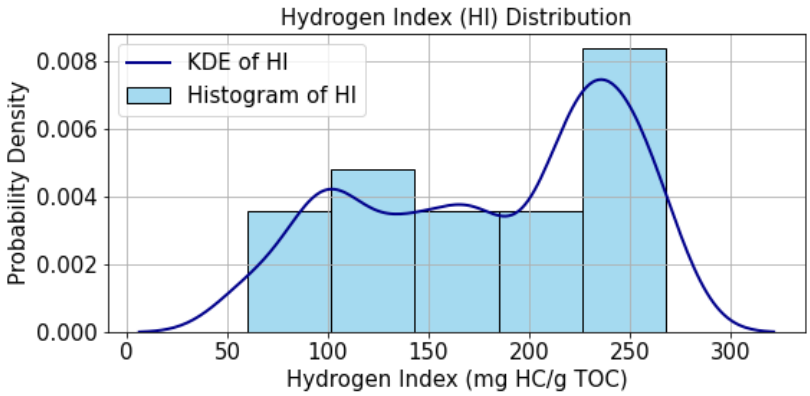

Figure 8. Data histogram and estimated distribution of Hydrogen Index (HI) from Rock-Eval pyrolysis data using KDE.

5.2.4 Boundary conditions

The basal thermal boundary condition is the paleo heat flow (HF), which is one of the most critical input parameters in basin modeling due to its significant impact on the amount, composition, and rate of petroleum generation (Hsu and Robinson, 2017).

In this study, paleo water depths (PWD) are estimated based on the depositional environment reported in the Western Australian Petroleum and Geothermal Information Management System

372 (WAPIMS) biostratigraphy database (Young et al., 2021; Tipsword et al., 1966). The minimum
373 and maximum PWD through geological time in the Canning Basin are shown in Figure 9.
374
375 The SWIT values are then calculated using the automatic SWIT tool in PetroMod, which derives
376 values based on PWD and the well location (Wygrala, 1989). The minimum and maximum SWIT
377 through geological time at the well location is presented in Figure 9.
378
379 The ranges of HF at different geological times are estimated based on the tectonic history, using
380 typical heat flow values reported by Allen and Allen (2005). A summary of the tectonic history is
381 provided in Table 4, while the estimated HF ranges over time are illustrated in Figure 9.
382
383 Boundary conditions are sampled only at the time points where depositional environment and
384 tectonic event data are available. These are assumed to follow a uniform distribution.
385
386 Table 4. Summary of tectonic history in the Canning Basin (Finder exploration, 2018)

Age	**Tectonic Event**
Late Cretaceous-Present Day	Tectonic quiescence
Early Cretaceous	Tectonic quiescence
End Jurassic	Regional uplift
Middle Jurassic	Tectonic quiescence and thermal subsidence
Middle Triassic-Middle Jurassic	Transgression
Early Triassic	Minor extension
Mid-Late Permian	End of glaciation

Early Permian	Major extension, rifting and subsidence
Early-Late Carboniferous	Alice Springs Orogeny equivalent
End Devonian	Major extension, rifting and rapid subsidence
Early-Mid Devonian	Continued compression, minor subsidence
End Silurian	Regional compression
Late Ordovician-Early Silurian	Thermal subsidence
Middle Ordovician	Rifting and thermal subsidence
Early Ordovician	NW-SW extension and rapid subsidence
Precambrian	

387

388

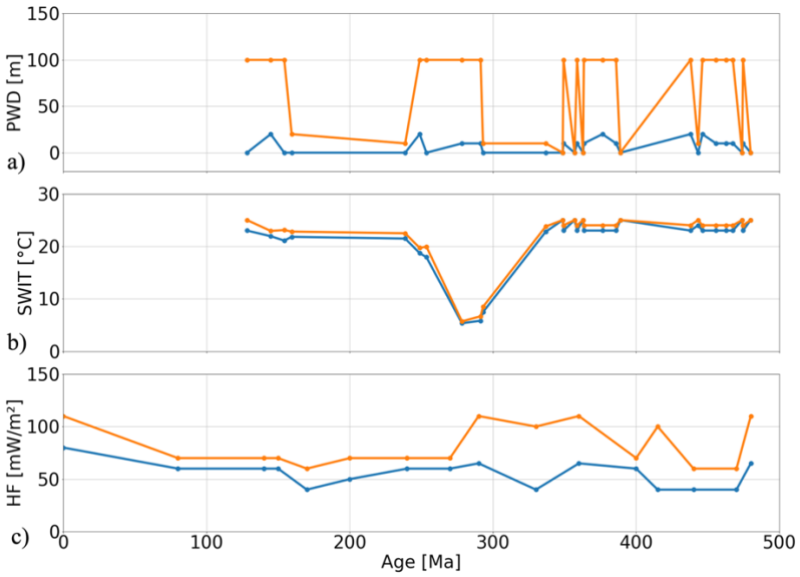

389

390 Figure 9. Estimated PWD, SWIT, and HF through geological time (Young et al., 2021; Finder
391 exploration, 2018). The orange and blue curves represent upper and lower bounds respectively.
392 The orange and blue dots are the estimated values based on the depositional environment.

393

5.3 Summary of Monte Carlo Sampling of uncertain parameters

Some of the uncertain parameters in the basin model are continuous variables, while others are categorical, such as the kinetic model type. For continuous variables, some can be resampled directly from the distributions of existing datasets, while others are defined only by estimated value ranges. As a result, different types of variables require different sampling strategies and underlying assumptions.

A summary of all the uncertain parameters, along with their corresponding sampling methods and data sources, is provided in Table 5.

Table 5. Summary of all the uncertain parameters and their sampling methods and data sources. KDE is kernel density estimation. DTMC is Discrete-Time Markov Chains.

Uncertain parameters	Distribution	Data source
Mineral compositions	Dirichlet distribution	Rock physics inversion
Porosity	KDE	Rock physics inversion
Paleo erosion	Truncated normal distribution	Sonic log
Kinetic model	DTMC	Rock-Eval pyrolysis data
TOC	KDE	Rock physics inversion
HI	KDE	Rock-Eval pyrolysis data
Boundary conditions	Uniform distribution	Depositional environment and tectonic history

6 Simulation setup

In the 1D basin model template, simulator options must be configured. Since the template was duplicated with only the input tables and boundary conditions modified, the simulation parameters remain consistent across all realizations. A total of 500 basin models were simulated.

A few simulation parameters were adjusted from their default values. The number of runs was set to 20 to ensure convergence of the iterative geometric optimization of layer thickness during forward modeling, while balancing computational time. The maximum cell thickness was set to 5 m, considering the minimum thickness interval of 7 m in Table 1, and the maximum time-step duration was reduced to 0.25 Ma to match the minimum age interval of 0.3 Ma in Table 1 and improve temporal resolution. Core measurements show that the Goldwyer III unit has very low matrix permeability (0.001–0.01 md) and porosity below 10%, consistent with tight shale systems (Finder Exploration, 2018). In such rocks, matrix-scale expulsion is likely limited and a substantial fraction of generated hydrocarbons may be retained in the pore network unless aided by natural fractures or strong overpressure (Jarvie, 2012; Sondergeld et al., 2010). Accordingly, for modeling purposes we assume low expulsion efficiency and apply a "generation-only" scenario with a 10% expulsion factor, while enabling "Organic secondary porosity", "Secondary cracking", and "Radiogenic heat" in the simulation.

7 Results

7.1 Sensitivity analysis of the model outputs to the uncertain inputs

Distance-based generalized sensitivity analysis (DGSA) is applied to evaluate how key uncertain parameters influence model outputs. (Fenwick et al., 2014; Park et al., 2016). The analysis focused on vitrinite reflectance, TR, temperature, and pore pressure within the Goldwyer III unit.

Since this sensitivity analysis algorithm only accepts scalar inputs, depth-varying and time-varying parameters such as porosity, TOC, HI, HF, and PWD are discretized into three representative categories: low, mid, and high, based on evenly divided value ranges. A categorical indicator is then assigned to each realization. For each category, the actual values at each depth or time step are sampled from the corresponding range using a uniform distribution. For input variables such as mineral compositions, which require the component fractions to sum to one, values at each depth are sampled from a Dirichlet distribution. To reduce dimensionality for the sensitivity analysis, the depth-averaged mineral compositions are used as representative scalar inputs. The kinetic model is treated as a categorical input, with a single model assigned uniformly across the full depth for each realization. Erosion magnitudes are directly sampled from their original distributions without further transformation.

This approach allows complex depth- and time-dependent parameters to be incorporated into the sensitivity analysis while preserving key aspects of their variability. A summary of all the input variables and their sampling strategies is list in Table 6.

Table 6. Summary of Input Variables and Sampling Strategies for Sensitivity Analysis.

Input variable	Type	Sampling method	Value range/ Categories	Notes

Porosity	Depth-varying	Categorical: [Low, Mid, High]	Equal thirds, p = [1/3, 1/3, 1/3]	Uniformly sampled within each range at each depth
TOC				
HI				
Mineral Compositions		Dirichlet distribution + Averaging	Posterior from inversion	Averaged across depth
Hydrocarbon generation kinetic Model		Random assignment	[Type II, Type III], p= [1/2, 1/2]	One model assigned to full column
Erosions	Scalar	Truncated normal distribution	From erosion maps	Sampled directly from fitted distribution
HF	Time-varying	Categorical: [Low, Mid, High]	Equal thirds, p = [1/3, 1/3, 1/3]	Time series simplified using category-based range
PWD				

A total of 500 basin models are simulated. The outputs within the Goldwyer III unit are extracted and used for sensitivity analysis. The key observations from Figure 10 are summarized below:

1. **Vitrinite reflectance**: Figure 10 shows that the two domain controls on thermal maturity are Cretaceous erosion and heat flow. This is because the timing and magnitude of erosion controls the maximum burial depth and corresponding peak temperature, which determine the maximum thermal maturity the source rock can achieve. Because vitrinite reflectance is an irreversible maturity indicator, erosion occurring near the time of maximum burial has a much stronger impact than earlier erosion (e.g., Triassic), as it can preserve the

462 maturity signal even if subsequent cooling occurs. Heat flow shows high sensitivity
463 because it directly controls the thermal gradient within the basin and significantly affects
464 the temperature evolution of the source rock. In contrast, the hydrocarbon generation
465 kinetic model appears to have limited influence on thermal maturity in this case. This is
466 because vitrinite reflectance is calculated using a separate kinetic model (Sweeney &
467 Burnham, 1990) that primarily depends on maximum temperature and exposure time,
468 rather than the kinetics of hydrocarbon generation.

469 2. **Transformation Ratio**: The sensitivity ranking in Figure 10 shows that transformation
470 ratio is most affected by Cretaceous erosion, kinetic model, and heat flow. Transformation
471 ratio reflects the extent and timing of kerogen cracking, which is governed by the basin's
472 thermal history (controlled by burial and heat flow) and the reaction kinetics assigned to
473 the kerogen (Pepper & Corvi, 1995). Since these factors control when kerogen starts to
474 crack and how fast it progresses, they have the largest impact on transformation ratio in
475 our results.

476 3. **Temperature**: Figure 10 shows that heat flow is the only sensitive parameter influencing
477 the present-day temperature profile. Variations in mineral composition within the
478 Goldwyer III unit have only a minor effect because heat is transferred mainly by
479 conduction from the basement upward. As a result, the present-day temperature is
480 controlled primarily by the heat-flow history and the thermal conductivity of the units
481 beneath the source rock, while lithologic variations within the source rock have a much
482 smaller impact on its current temperature.

483 4. **Pore pressure**: Figure 10 shows that pore pressure is most sensitive to porosity, erosion
484 magnitude, TOC, and key mineral components such as quartz and calcite. Porosity has a

strong influence because it directly controls pore volume and fluid retention capacity, which affects pressure buildup during burial. Erosion impacts pore pressure because it changes the maximum burial depth and subsequent exhumation, which in turn governs compaction trends. TOC contributes to overpressure because hydrocarbon generation during maturation leads to fluid expansion and kerogen-to-hydrocarbon transformation. Mineral composition also matters because quartz-rich rocks are mechanically stronger and more resistant to compaction, helping to preserve pore space at depth, whereas calcite-rich rocks deform more easily and are susceptible to pressure solution, resulting in greater porosity loss and higher pore pressures.

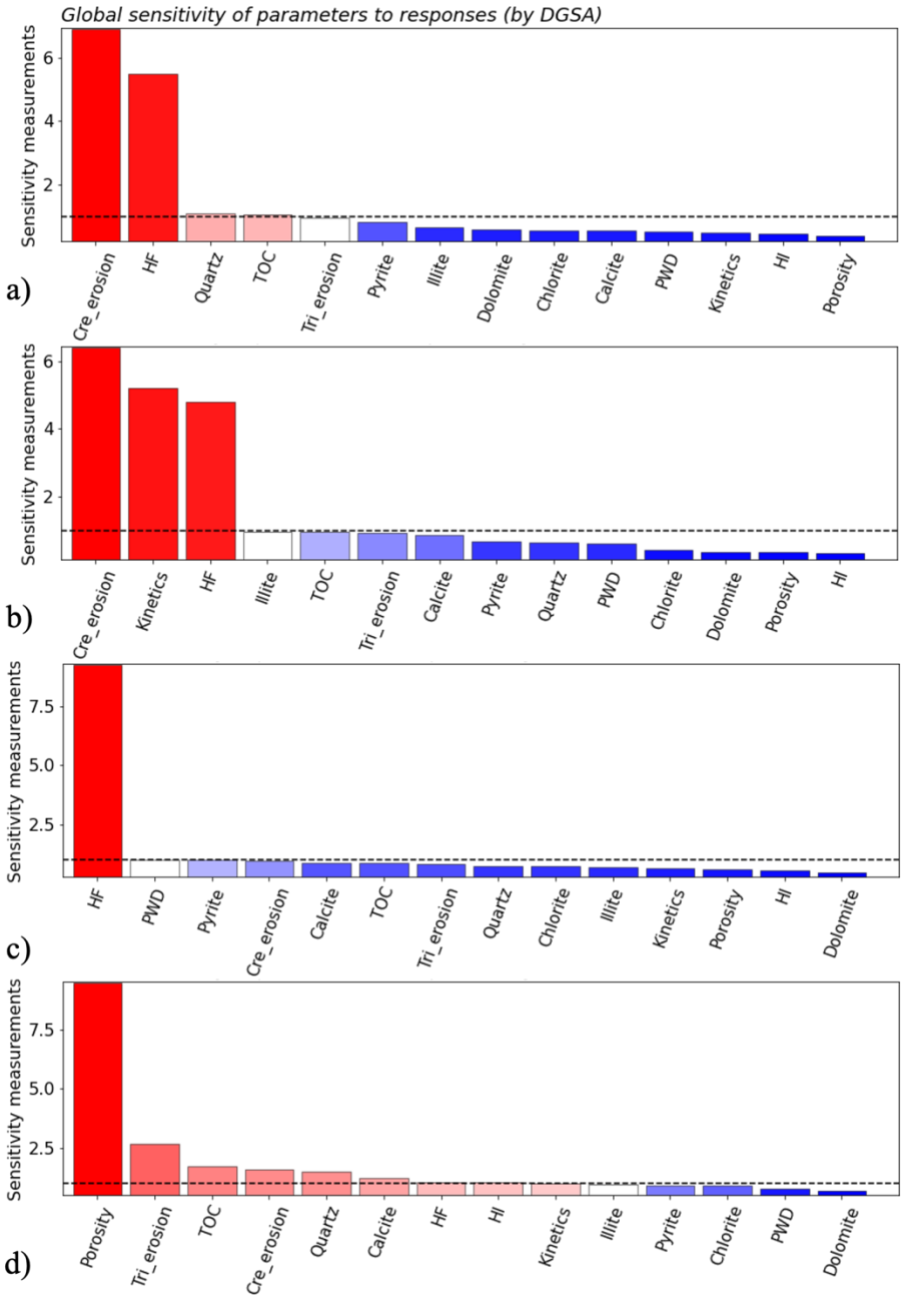

Figure 10. Results of Distance-based Generalized Sensitivity Analysis (DGSA) for key model outputs. Each panel shows the relative importance of uncertain input parameters in influencing the output variable: (a) Vitrinite reflectance, (b) Transformation ratio (TR), (c) Temperature, (d) Pore pressure. Sensitivity is measured using distance-based metrics across categorized input realizations. Bars represent the contribution of each input to output variability. Cre_erosion is

Cretaceous erosion. Tri_erosion is Triassic erosion. HF is heat flow. TOC is total organic carbon. PWD is paleo water depth. HI is hydrogen index.

7.2 Summary of basin model outputs from Monte Carlo simulation

A new set of 500 basin model realizations was generated for the summary analysis in Section 7.2, independent from the DGSA sample set in Section 7.1. This is because, in Section 7.1, certain depth- and time-dependent input parameters were transformed into scalar or categorical forms to meet the requirements of the DGSA algorithm. As a result, those realizations do not fully preserve the continuous variability of the original inputs. In contrast, the realizations in Section 7.2 were generated using the original, non-discretized input parameter distributions to better capture the full range of model behavior and variability in the Monte Carlo outputs.

The depth-dependent distributions of vitrinite reflectance, TR, temperature, and pore pressure are shown in Figure 11. The wide variability among realizations arises from the stochastic sampling of posterior petrophysical inputs, erosion magnitudes, thermal boundary conditions, and organic facies properties. Because these parameters strongly influence mechanical compaction, thermal evolution, hydrocarbon generation, and pressure development, their combined uncertainty propagates through the Monte Carlo basin modeling, resulting in substantial variability in the simulated results. The key observations are summarized below:

1. **Vitrinite reflectance**: Vitrinite reflectance increases with depth across all realizations. Within the Goldwyer III unit, the vitrinite reflectance range from 0.7 $\%R_o$ to 1.5 $\%R_o$, wth

an interquartile range is between 0.8 $\%R_o$ to 1.1 $\%R_o$. These values fall within the oil window (~0.5 $\%R_o$ to ~1.0 $\%R_o$) and wet gas window (~1.0 $\%R_o$ to ~1.4 $\%R_o$) (Kibria et al., 2020). The uncertainty of vitrinite reflectance widens at greater depths, primarily due to erosion magnitude and thermal boundary condition. These two factors control the basin's past temperature history, which leads to a wider range of possible vitrinite reflectance values at depth.

2. **Transformation Ratio (TR)**: TR increases with depth and shows significant variability within the Goldwyer III unit. Across all realizations, TR ranges from 10% to 90%, with an interquartile range between 50% and 80%. The median value is approximately 70%, indicating substantial but incomplete transformation across most realizations.
3. **Temperature**: Temperature uncertainty increases gradually with depth. The median temperatures at the top and base of the Goldwyer III unit are approximately 95 $°C$ and 100 $°C$, respectively. The narrow interquartile range indicate relatively low thermal uncertainty compared to maturity and TR outputs. The bottom hole temperature measurement fails within the interquartile range (25^{th} –75^{th} percentile), further supporting the consistency of the modeled temperature.
4. **Pore pressure**: Pore pressure simulations show less variability than other outputs. Above the Goldwyer III unit, most of the realizations remain near hydrostatic condition. Within the Goldwyer III unit, the pore pressure shows slightly larger variability, but the interquartile range remains narrow. This is because pore pressure is primarily controlled by mechanical compaction, permeability, and hydrocarbon generation, and both compaction and permeability are functions of porosity. In our Monte Carlo setup, only the porosity within the Goldwyer III unit is sampled from the inversion, which limits the range

of pressure outcomes. As a result, pore pressure is less sensitive to uncertainty in the other input variables and shows smaller variability than the other modeled outputs.

Overall, vitrinite reflectance and TR exhibit the highest sensitivity to uncertain inputs, while temperature and pore pressure remains less variable across the realizations.

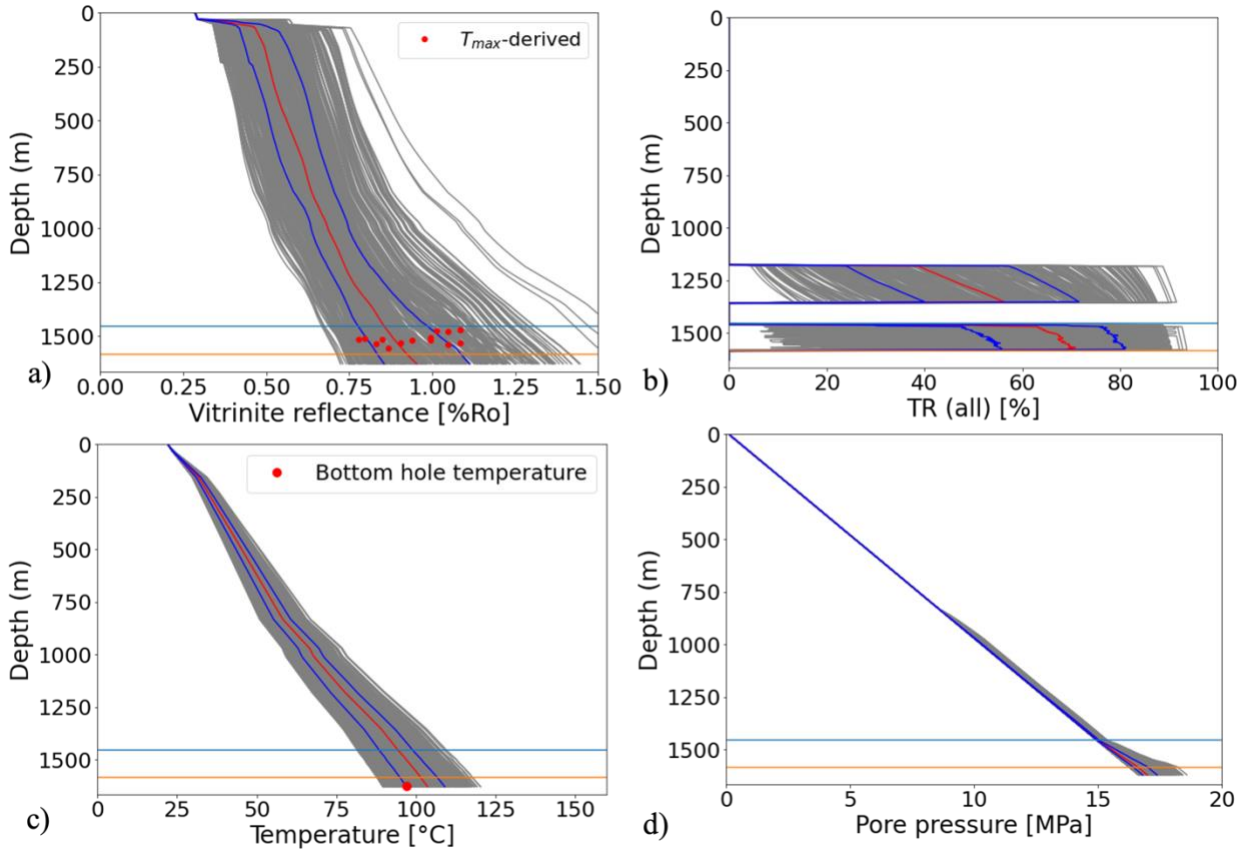

Figure 11. Monte Carlo simulations of vitrinite reflectance (thermal maturity), transformation ratio (TR), temperature, and pore pressure. The grey curves represent individual realizations from the basin model simulations. The dark blue curves indicate the 25th and 75th percentiles, while the red curves show the median. The light blue and light orange curves represent the top and bottom boundaries of the Goldwyer III unit, respectively. The red dots in the vitrinite reflectance plot are

559 calculated using a T_{max}-based empirical correlation (Jarvie, 2001). The red dot in the temperature
560 plot represents the bottom-hole temperature.
561
562 **8 Discussion**
563 **8.1 Uncertainty reduction in thermal maturity**
564
565 One of the key advantages of the Monte Carlo basin modeling approach is its ability to reduce the
566 uncertainty in thermal maturity estimates by incorporating uncertainty of geological history,
567 petrological inputs, and physical constraints. To evaluate this, we compare vitrinite reflectance
568 estimated from three different methods: (1) Monte Carlo basin modeling in this study; (2) rock
569 physics inversion which estimates maturity based on present-day petrophysical and seismic
570 signatures (Huang et al., 2025); (3) T_{max}-based empirical calculation, which uses geochemical
571 measurements to estimate vitrinite reflectance (Jarvie, 2001).
572
573 Figure 12 shows that all the T_{max}-derived vitrinite reflectance values fall within the range of
574 realizations from the Monte Carlo basin modeling and most of the values lie within the interquartile
575 range of the simulation results, indicating strong agreement. The distribution plot further illustrates
576 that the posterior distribution of vitrinite reflectance from the rock physics inversion shows limited
577 updating with respect to its prior, while the distribution from the Monte Carlo basin modeling is
578 narrower and closely aligns with the calculated vitrinite reflectance values. This reduction in
579 uncertainty reflects the additional geological constraints introduced by the forward modeling
580 process that incorporates the geohistory of the basin in addition to rock physics and seismic
581 signatures.

These results demonstrate that Monte Carlo basin modeling improves confidence in thermal maturity predictions, which is a significant advantage for hydrocarbon generation assessments and risk reduction in exploration.

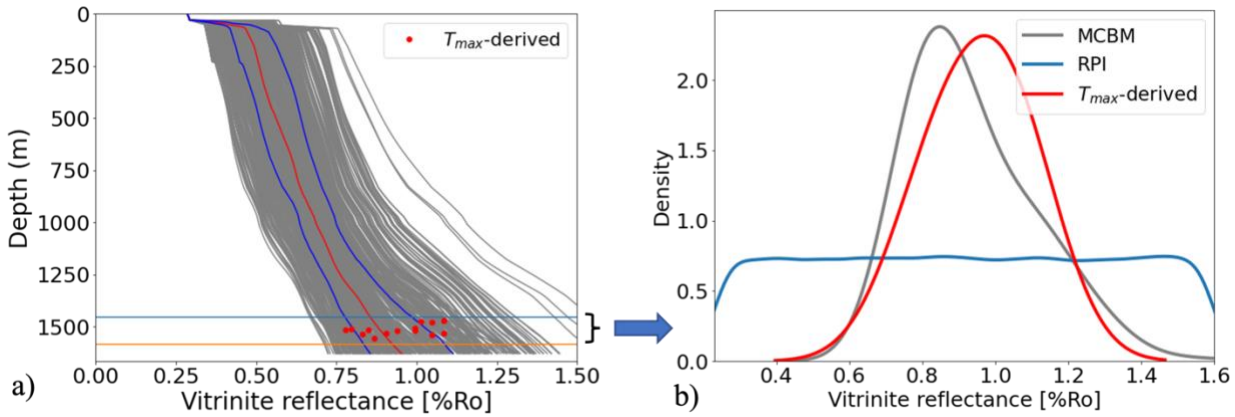

Figure 12. Comparison of vitrinite reflectance from different sources. a). Monte Carlo basin modeling and T_{max}-derived vitrinite reflectance. The grey curves represent individual realizations from the basin model simulations. The dark blue curves indicate the 25th and 75th percentiles, while the red curves show the median. The light blue and light orange curves represent the top and bottom boundaries of the Goldwyer III unit, respectively. The red dots are the T_{max}-derived vitrinite reflectance. b). Distributions of vitrinite reflectance within the Goldwyer III unit from Monte Carlo basin modeling (grey curve), posterior of rock physics inversion (blue curve), and T_{max}-based calculation (red curve).

8.2 Limitations

Despite these strengths, there are several limitations in this study. Firstly, there are no calibration data such as pressure measurements or lab measured vitrinite reflectance. Incorporating such data in future studies could further reduce uncertainty in source rock property estimates. Second, although the Monte Carlo framework allows for comprehensive uncertainty quantification, the overall workflow remains computationally intensive. While the simulation itself runs efficiently, performance bottlenecks occur during the editing, saving, and loading of lithology configurations and output files. Further optimization is needed to improve data handling efficiency and streamline the modeling process. Third, the current implementation uses 1D basin models. Extending the approach to 2D or 3D models in future work could better capture spatial heterogeneity and improve the accuracy and reliability of the results, at more computational cost.

9 Conclusion

This study presents a comprehensive Monte Carlo basin modeling framework that can incorporate uncertainties in petrological inputs, paleo-erosion magnitudes, organic facies properties, and boundary conditions to quantify key source rock properties, including vitrinite reflectance, transformation ratio, temperature, and pore pressure.

The simulation results (Figure 11) show that the source rock within the Goldwyer III unit in the study area is in the oil or wet gas window with substantial but incomplete transformation. Sensitivity analysis (Figure 10) indicates that Cretaceous erosion and heat flow are the dominant factors influencing thermal maturity. The transformation ratio also shows strong sensitivity to the hydrocarbon generation kinetic model, highlighting the importance of selecting appropriate kinetic

parameters when evaluating hydrocarbon generation potential. A comparison of thermal maturity results (Figure 12) from Monte Carlo basin modeling, rock physics inversion, and Tmax-based empirical methods demonstrates that the Monte Carlo approach significantly reduces uncertainty. The basin modeling outputs not only align well with geochemical maturity indicators but also exhibit narrower distributions compared to rock physics inversion, reflecting the added value of incorporating geological and physical constraints.

Overall, this integrated framework improves the robustness and reliability of source rock property predictions and provides a valuable workflow for source rock evaluation, risk assessment, and decision-making in hydrocarbon exploration.

Acknowledgement

This work is supported by the funding from the sponsors of the Stanford Center for Earth Resources Forecasting (SCERF) and Stanford Natural Gas Initiative (NGI). We thank Western Australia's Department of Mines, Industry Regulations and Safety for providing the necessary data used in this study. We would also like to acknowledge Lukman Mobolaji Johnson for his thoughtful discussion.

Reference

Al Ibrahim, M. (2019). *Petroleum system modeling of heterogeneous organic-rich mudrocks*. Stanford University. GitHub site: : https://github.com/MosGeo/BPSMAutoToolbox

Al Ibrahim, M. A., Mukerji, T., & Scheirer, A. H. (2020, February). A thermal-maturation dependent elastic rock physics template for organic-rich mudrocks: Construction and application. In *Fifth EAGE workshop on rock physics* (Vol. 2020, No. 1, pp. 1-5). European Association of Geoscientists & Engineers.

Allen, P. A., & Allen, J. R. (2005). Basin analysis: Principles and applications (2nd ed.). Blackwell Publishing.

Allen, P. A., & Allen, J. R. (2013). *Basin analysis: Principles and application to petroleum play assessment*. John Wiley & Sons.

Athy, L. F. (1930). Density, porosity, and compaction of sedimentary rocks. *Aapg Bulletin*, *14*(1), 1-24.

Brevik*, I., Szydlik, T., Corver, M. P., De Prisco, G., Stadtler, C., & Helgesen, H. K. (2014). Geophysical basin modeling: Generation of high quality velocity and density cubes for seismic imaging and gravity field monitoring in complex geology settings. In *SEG Technical Program Expanded Abstracts 2014* (pp. 4733-4737). Society of Exploration Geophysicists.

Brown, S. A., Boserio, I. M., Jackson, K. S., & Spence, K. W. (1984). The geological evolution of the Canning Basin-implications for petroleum exploration.

Cadman, S., Pain, L., Vuckovic, V., & Le Poidevin, S. (1993). *Canning Basin* (Vol. 9). Australian Petroleum Accumulations Report, Western Australia, 81 pp.

D'Ercole, C., Gibbons, L., & Ghori, K. A. R. (2003). *Prospects and leads, central Canning Basin, Western Australia, 2003* (Record 2003/14). Western Australia Geological Survey.

Fenwick, D., Scheidt, C., & Caers, J. (2014). Quantifying asymmetric parameter interactions in sensitivity analysis: application to reservoir modeling. *Mathematical Geosciences*, *46*, 493-511.

Finder Exploration. (2018). Maturity and unconventional resource modelling: April 2018 update for Finder Exploration's Pan-Canning Goldwyer unconventional limit project (PC-GULP) [PowerPoint slides]. Finder Exploration. (https://wapims.dmp.wa.gov.au/WAPIMS/)

Fonseca, J., Pradhan, A., & Mukerji, T. (2023). Bayesian geophysical basin modeling with seismic kinematic metrics to quantify uncertainty for pore pressure prediction. *Geophysics*, *88*(6), M239-M259.

Foster, C. B., O'Brien, G. W., & Watson, S. T. (1986). Hydrocarbon source potential of the Goldwyer Formation, Barbwire terrace, Canning basin, western Australia. *The APPEA Journal*, *26*(1), 142-155.

690 Ghori, K. A. R., & Haines, P. W. (2007). Paleozoic petroleum systems of the Canning Basin,
691 Western Australia: a review. *Search and Discovery*, *5*.
692
693
694 Garcia, M. P. (2014). Tectonic evolution and source rock maturation, Canning Basin, Western
695 Australia.
696
697
698 Haines, P. W. (2004). *Depositional facies and regional correlations of the Ordovician Goldwyer*
699 *and Nita Formations, Canning Basin, Western Australia, with implications for petroleum*
700 *exploration* (Record 7). Geological Survey of Western Australia.
701
702 Haines, P. W. (2011). Geology, exploration history, and petroleum prospectivity of state acreage
703 release area L11-5, Canning Basin, Western Australia. *Perth: Geological Survey of Western*
704 *Australia*, 1-10.
705
706 Hantschel, T., & Kauerauf, A. I. (2009). *Fundamentals of basin and petroleum systems modeling*.
707 Springer Science & Business Media.
708
709 Hsu, C. S., & Robinson, P. R. (Eds.). (2017). *Springer handbook of petroleum technology*.
710 Springer.
711
712 Huang, J., Scheirer, A. H., & Mukerji, T. (2025). Statistical rock physics inversion for assessing
713 source rock potentials from seismic signatures: An application to the Canning Basin, Australia.
714 EarthArXiv. https://doi.org/10.31223/X5R15G

Iqbal, M. A., Rezaee, R., Laukamp, C., Pejcic, B., & Smith, G. (2022). Integrated sedimentary and high-resolution mineralogical characterisation of Ordovician shale from Canning Basin, Western Australia: Implications for facies heterogeneity evaluation. *Journal of Petroleum Science and Engineering*, *208*, 109347.

Jarvie, D. M., Claxton, B. L., Henk, F., & Breyer, J. T. (2001, June). Oil and shale gas from the Barnett Shale, Fort Worth basin, Texas. In *AAPG annual meeting program* (Vol. 10, p. A100).

Jarvie, D. M., 2012, Shale resource systems for oil and gas: Part 2 — Shale-oil resource systems, in J. A. Breyer, ed., Shale reservoirs — Giant resources for the 21st century: AAPG Memoir 97, p. 89 – 119.

Johnson, L. M. (2019). *Integrated Reservoir Characterization of the Goldwyer Formation Canning Basin* (Doctoral dissertation, Curtin University).

Johnson, L. M., Rezaee, R., Kadkhodaie, A., Smith, G., & Yu, H. (2017). A new approach for estimating the amount of eroded sediments, a case study from the Canning Basin, Western Australia. *Journal of Petroleum Science and Engineering*, *156*, 19-28.

Johnson, L. M., Rezaee, R., Smith, G. C., Mahlstedt, N., Edwards, D. S., Kadkhodaie, A., & Yu, H. (2020). Kinetics of hydrocarbon generation from the marine Ordovician Goldwyer Formation, Canning Basin, Western Australia. *International Journal of Coal Geology*, *232*, 103623.

Kibria, M. G., Das, S., Hu, Q. H., Basu, A. R., Hu, W. X., & Mandal, S. (2020). Thermal maturity evaluation using Raman spectroscopy for oil shale samples of USA: comparisons with vitrinite reflectance and pyrolysis methods. *Petroleum Science*, *17*, 567-581.

Kuuskraa, V., Stevens, S. H., & Moodhe, K. D. (2013). Technically recoverable shale oil and shale gas resources: An assessment of 137 shale formations in 41 countries outside the United States (Report). U.S. Energy Information Administration. https://www.eia.gov/analysis/studies/worldshalegas/pdf/overview.pdf

MacKay, D. J. (2003). *Information theory, inference and learning algorithms*. Cambridge university press.

Minka, T. (2000). *Estimating a Dirichlet distribution*.

Norris, J. R. (1998). *Markov chains* (No. 2). Cambridge university press.

Park, J., Yang, G., Satija, A., Scheidt, C., & Caers, J. (2016). DGSA: A Matlab toolbox for distance-based generalized sensitivity analysis of geoscientific computer experiments. *Computers & geosciences*, *97*, 15-29.

Pepper, A. S., & Corvi, P. J. (1995). Simple kinetic models of petroleum formation. Part I: oil and gas generation from kerogen. *Marine and petroleum geology*, *12*(3), 291-319.

761

762 Peters, K. E., & Cassa, M. R. (1994). Applied source rock geochemistry.

763

764 Peters, K. E., Curry, D. J., & Kacewicz, M. (2012). An overview of basin and petroleum system

765 modeling: Definitions and concepts.

766

767 Schenk, C. J., Tennyson, M. E., Mercier, T. J., Woodall, C. A., Finn, T. M., Le, P. A., ... &

768 Leathers-Miller, H. M. (2018). *Assessment of undiscovered oil and gas resources in the Canning*

769 *Basin Province, Australia, 2017* (No. 2018-3023). US Geological Survey.

770

771 Sondergeld, C. H., Newsham, K. E., Comisky, J. T., Rice, M. C., & Rai, C. S. (2010, February).

772 Petrophysical considerations in evaluating and producing shale gas resources. In *SPE*

773 *Unconventional Resources Conference/Gas Technology Symposium* (pp. SPE-131768). SPE.

774

775 Sweeney, J. J., & Burnham, A. K. (1990). Evaluation of a simple model of vitrinite reflectance

776 based on chemical kinetics. *AAPG bulletin*, *74*(10), 1559-1570.

777

778 Tipsword, H. L., Setzer, F. M., & Smith Jr, F. L. (1966). Interpretation of depositional environment

779 in Gulf Coast petroleum exploration from paleoecology and related stratigraphy.

780

781 Tong, Y., & Mukerji, T. (2017). Generalized sensitivity analysis study in basin and petroleum

782 system modeling, case study on Piceance Basin, Colorado. *Journal of Petroleum Science and*

783 *Engineering*, *149*, 772-781.

Tømmerås, A., Sylta, Ø., Daszinnies, M. C., & Mencaroni, D. (2018). Prewell and postwell predictions of oil and gas columns using an iterative Monte Carlo technique with three-dimensional petroleum systems modeling. *AAPG Bulletin*, *102*(4), 709-728.

Virtanen, P., Gommers, R., Oliphant, T. E., Haberland, M., Reddy, T., Cournapeau, D., ... & Van Mulbregt, P. (2020). SciPy 1.0: fundamental algorithms for scientific computing in Python. *Nature methods*, *17*(3), 261-272.

Young, A., Flament, N., Hall, L., & Merdith, A. (2021). The influence of mantle flow on intracontinental basins: Three examples from Australia. *Basin Research*, *33*(2), 1429-1453.

Wygrala, B. P. (1989). Integrated study of an oil field in the southern Po basin, northern Italy.
Young, A., Flament, N., Hall, L., & Merdith, A. (2021). The influence of mantle flow on intracontinental basins: Three examples from Australia. *Basin Research*, *33*(2), 1429-1453.